Full Paper

Journal of the Brazilian Chemical Society

https://dx.doi.org/10.21577/0103-5053.20250170

J. Braz. Chem. Soc. **2026**, *37*, e-20250170, 1-10

Promoting Osteoblast Proliferation and Activity by Combining Natural Rubber Hybrid Systems with Calcium Phosphate and Silica Particles

Luciana M. da Silva,[,a] Rodney M. do Nascimento,[b,c] Naiara C. Oliveira,[d] Beatriz O. Lopes,[e] Ana Caroline R. M. Leite,[e] Mirna M. Bezerra,[a] Renata F. C. Leitão,[a] Francisco Airton C. da Rocha,[f] Amauri J. de Paula[g,h] and Virgínia C. C. Girão-Carmona[a]*

[a]*Departamento de Morfologia, Faculdade de Medicina, Universidade Federal do Ceará, 60430-170 Fortaleza-CE, Brazil*

[b]*Instituto Federal de Santa Catarina, 88040-900 Florianópolis-SC, Brazil*

[c]*DvDt Startec: Research, Development and Training, 3690-000 Descalvado-SP, Brazil*

[d]*Departamento de Física, Universidade Regional do Cariri, 63041-145 Juazeiro do Norte-CE, Brazil*

[e]*Universidade da Integração Internacional da Lusofonia Afro-Brasileira, 62790-000 Redenção-CE, Brazil*

[f]*Programa de Pós-Graduação em Ciências Médicas, Faculdade de Medicina, Universidade Federal do Ceará, 60430-170 Fortaleza-CE, Brazil*

[g]*Grupo de Interfaces Sólido-Biológicas (SolBIN), Departamento de Física, Universidade Federal do Ceará, 60455-900 Fortaleza-CE, Brazil*

[h]*Ilum Escola de Ciências, Centro Nacional de Pesquisa em Energia e Materiais (CNPEM), 13087-548 Campinas-SP, Brazil*

Natural rubber (NR) latex from *Hevea brasiliensis* can be modified with functional particles to obtain advanced materials. This study evaluates the biocompatibility of two NR-based hybrid systems incorporating calcium phosphate (CaP) and silica (SiP) particles for medical and industrial use. Films (NRHS) were prepared using chloroform (CHF) and toluene (TOL) as solvents, and their physicochemical surface properties and interactions with osteoblastic cells were analyzed. Parameters included morphology, alkaline phosphatase (ALP) activity, and cell viability ((3-(4,5-dimethylthiazol-2-yl)-2,5-diphenyl tetrazolium bromide (MTT) assay). Hybridization altered surface energy and wettability, key factors for biocompatibility. Depending on solvent and particle combinations, NRHS modulated osteoblast responses, either preserving, impairing, or enhancing proliferation and enzymatic activity. Both NR-CaP and NR-SiP composites influenced surface energy and contact angle, while generally maintaining viability. These results highlight the tunability of NRHS via particle incorporation, and their positive cellular interactions suggest strong potential for biosensing and biomedical device engineering.

Keywords: natural polymer, functional nanoparticles, surface wettability, osteoblast cell

Introduction

In recent years, the exploration of biomaterials from diverse natural sources - including alginate, chitosan, animal-derived collagen, and plant-based compounds such as cellulose - has intensified, driven by the growing demand for non-toxic, sustainable, and functional materials in healthcare. Among these, natural rubber (NR), harvested from *Hevea brasiliensis*, has been the subject of extensive research due to its potential for enhancement when combined with various materials, yielding improvements in electromechanical properties,[1-3] thermal conductivity, mechanical strength,[4] hydrophilicity,[5] and flame-retardant properties.[6,7] Natural biocompatibility makes NR an attractive alternative for biological and medical

*e-mail: lumascena2@gmail.com
Editor handled this article: Célia M. Ronconi (Associate)

applications. However, processes for hybridizing NR with other polymers and particles necessitate extensive research to determine how the resulting physicochemical properties influence biocompatibility, particularly for applications in the medical field.

The incorporation of novel components in the natural polymer matrix can alter this characteristic by modifying the internal and surface features of the material.[8,9] As a consequence, its biocompatibility can also be modified. Modifying surface characteristics, including wettability and surface energy, is recognized to have a considerable impact on cellular response[10,11] and is thus a critical aspect of NR composites for medical applications. For instance, NR and calcium phosphate (CaP) are combined in the NR-CaP hybrid system, which has shown promise in tissue regeneration, in particular due to the mechanical properties of the NR as a cell substrate,[12] and the capability to stimulate bone regeneration, create apatite, and exhibit osteogenic differentiation *in vitro*.[13,14] Herein, NR-CaP samples were developed and characterized with the aim of applications as a calcium phosphate gradual release composite. Likewise, silica particles (SiP) have been widely employed as fillers in NR-SiP to enhance the mechanical[15,16] and thermal attributes[17,18] of biopolymers. In addition, by employing silica particles as probes, it is possible to evaluate chemical stability even under high ionic strength and shear stress, suggesting promising potential for NR coatings in fields such as medicine, microelectronics, and the automotive sector.[19] On the other hand, there is a controversy in terms of cell response concerning silica particles. Cell viability experiments indicated that low particle doses of amorphous silica induced a small nonsignificant reduction in cell viability compared to crystalline silica which led to increased levels of toxicity,[20] while research indicates that SiP has been associated with osteogenic effects through the induction of gene expression for bone markers,[21] regulation of alkaline phosphatase (ALP) expression,[22] and enhancement of mineralization.[23] Herein, NR-SiP samples were developed and characterized to act as a probe system to evaluate chemical stability in release composites.

This paper describes the effects of NR hybrid system films (NRHS) incorporating CaP and SiP, and the impact of changing solvent types used during system synthesis, on osteoblastic cells for their prospective applications in bone tissue engineering and biosensing. The NRHS processing was monitored through contact angle measurements to evaluate the physicochemical properties of the material surfaces (particularly wettability and surface energy), as well as optical characterization to assess the subsequent impact on murine osteoblastic proliferation, activity, and viability. Taking into account the influence of solvent, furthermore, given that the surface charge of SiP can be manipulated, we also investigated the effects of negatively and positively charged SiP on the morphology of the NR matrix and its subsequent influence on cell dynamics. The results are divided into three topics: the first focuses on the science and engineering involved in the production of the NR-CaP, while the second focuses on the NR-SiP. In both topics, qualitative and quantitative data related to physicochemical and biological aspects are reported. The final topic presents the variability of cellular morphologies that can be obtained by the NR composites. The hybrid NR systems developed in our study capitalize on the distinctive properties of NR and are poised to be a viable biomaterial for applications in medical fields.

Experimental

Materials

Calcium nitrate tetrahydrate ($Ca(NO_3)_2{\cdot}4H_2O$, 99%), orthophosphoric acid (H_3PO_4, ≥ 85 wt.% in H_2O), ethylene glycol ($HOCH_2CH_2OH$, 99.8%), methyl alcohol (CH_3OH, 99.5%), ammonium hydroxide (NH_4OH, 28-30%) and chloroform ($CHCl_3$, 99%), acquired from Sigma-Aldrich (St. Louis, MO, USA), were used for the production of the bioactive ceramic powders based on CaP. Tetraethyl orthosilicate (TEOS, 98%), (3-aminopropyl) trimethoxysilane (APTMS, 97%), and fluorescein isothiocyanate (FITC, 97.5%) were from Sigma-Aldrich (St. Louis, MO, USA), ammonium solution (NH_4OH, 28-30%) was from Vetec (Rio de Janeiro, RJ, Brazil), absolute ethanol (EtOH, 99.5%) was from Dinâmica (Indaiatuba, SP, Brazil), and ultra-pure water from a Milli-Q® Direct Water Purification System (EMD Millipore, Burlington, MA, USA) were used for the production of the SiP. Raw NR latex was collected from *Hevea brasiliensis* trees (clone RRIM 600) at Estância Regina farm, State of São Paulo, Brazil (20º33'21.03''S 48º61'13.49''W) and immediately placed in propylene tubes containing 0.9% m/m ammonia and stored under at 4 °C to avoid microbial contamination.

Preparation of the NR suspensions

A volume of 1.5 mL from the raw latex suspension was transferred into 2 mL microcentrifuge tubes. The samples were then centrifuged for 90 min at 24 °C using an Eppendorf 5418 R centrifuge to facilitate phase separation and obtain the NR cream phase. The centrifugation was performed at a speed of 14,000 rcf. Post-centrifugation, the cream phase was extracted using a spatula and subsequently

dried in a controlled environment at 45 ºC for 24 h. The dried NR was then re-dispersed in chloroform and toluene to achieve a final concentration of 10 mg mL^{-1}, and namely CHF and TOL samples, respectively, to refer to NR prepared with these solvents. Following this, 100 µL of each NR suspension (in both solvents) were evenly applied onto glass coverslips and left to dry at ambient temperature.

Production of NR-CaP hybrid films

Calcium phosphate (CaP) was synthesized via a sol-gel process, employing calcium nitrate tetrahydrate and orthophosphoric acid as the starting materials, mixed in an 80:20 wt.% ratio.[11] These precursors were dissolved in a 15 mL mixture of methyl alcohol and ethylene glycol, maintaining a 2:1 volume ratio. The resultant solution was subjected to magnetic stirring at room temperature for 1 h to form a sol. The subsequent aging of the sol was carried out for 24 h at 50 °C with continuous magnetic stirring, yielding an opaque and viscous gel. This gel was then dried at 100 °C for 1 h and manually ground into a fine powder using a mortar and pestle. The powder underwent annealing at 700 °C for 1 h and was then stored at room temperature. The methodology for generating the CaP powder as outlined above has been previously developed by our research team.[24] Bioactive ceramic powders based on CaP, containing 47.8% Ca_5P_8, 9.5% Ca $(PO_4)_3OH$, 36.3% $CaCO_3$, and 6.3% Ca, were dispersed in the solvents at a concentration of 0.1 mg mL^{-1} and sonicated for 30 min to ensure proper dispersion. Following this step, the resulting suspensions were combined with the natural rubber (NR) solution in a 9:1 weight ratio (NR:CaP), based on the solid content. The final mixture was then subjected to magnetic stirring for 30 min. Subsequently, 100 µL of the resultant NR-CaP suspensions in chloroform (CHF-CaP) and toluene (TOL-CaP) were precisely deposited onto glass coverslips and allowed to dry at ambient temperature. The final CaP concentration within the NR-CaP hybrid films for both CHF-CaP and TOL-CaP samples was established at 0.2 mg mL^{-1}.

Production of NR-SiP hybrid films

Fluorescent spherical SiP were synthesized using a modified Stöber method.[25] To fabricate negatively charged SiP, 3.0 mg of fluorescein isothiocyanate (FITC) were initially dissolved in 3 mL of absolute ethanol, followed by the addition of 3.2 µL of (3-aminopropyl) trimethoxysilane (APTMS). The mixture was gently mixed and allowed to react for 1 h at room temperature in the dark. Subsequently, 1.5 mL of absolute ethanol, 800 µL of tetraethyl orthosilicate (TEOS), and 6.3 mL of ammonium hydroxide (NH_4OH) were added to the mixture. The reaction was conducted with stirring at 60 °C for 2 h. The product was then centrifuged at 48,200 rcf at 4 °C for 30 min to remove excess reagents. The supernatant was discarded, and the pellet was re-dispersed in absolute ethanol, followed by sonication in an ultrasonic bath (Cole-Parmer, IL, USA). This centrifugation and re-dispersion cycle was repeated three times. The concentration of the negatively charged SiP was quantified using thermogravimetric analysis. For the synthesis of positively charged SiP, amino functionalization was carried out using a post-grafting method.[26] A solution containing 28 µL of APTMS, 63 µL of NH_4OH, and 100 µL of ultrapure water was gradually introduced to 12 mL of a 20 mg mL^{-1} SiP suspension under vigorous stirring. The mixture was then stirred and refluxed at 75 °C for 3 h to facilitate covalent binding of APTMS to the SiP surface. Post-reaction, the suspension underwent centrifugation at 48,200 rcf at 4 °C for 30 min to eliminate any unreacted reagents. The supernatant was discarded, and the resultant positively charged SiP were re-suspended in absolute ethanol using an ultrasonic bath (Cole-Parmer, IL, USA). This centrifugation and re-suspension sequence was performed three times. The concentration of the positively charged SiP was also determined by thermogravimetric analysis. To prevent aggregation of SiP (both negatively and positively charged) during the preparation of the NR hybrids, they were sonicated prior to being combined with the NR suspension in either chloroform or toluene. Afterward, 100 µL of the NR-SiP suspensions were carefully deposited onto glass coverslips and left to dry at ambient temperature. The final concentration of SiP within the NR-SiP hybrid films was established at 0.1 mg mL^{-1}. The NR hybrid films were denominated based on the solvent used for the NR suspension and the surface charge of the SiP: chloroform and silica (CHF-Si), chloroform and aminofunctionalized silica (CHF-ASi), toluene and silica (TOL-Si), and toluene and aminofunctionalized silica (TOL-ASi) samples.

Microscopic characterization of the NR hybris films

The spatial distribution of CaP and SiP within the NR-based hybrid films was assessed using a confocal laser scanning microscope (CLSM; Zeiss LSM 710, Munich, Germany). Imaging was performed employing a 100× Zeiss EC Plan-Neofluor objective lens with a numerical aperture (NA) of 1.3, a working distance of 0.20 mm, and using oil immersion. A 405 nm laser was employed to visualize the NR and NR-CaP components, while a 488 nm laser was used to excite the FITC encapsulated in the SiP cores.

Surface characterization by contact angle measurements

Static contact angle measurements were conducted using a Ramé-Hart 250-F1 tensiometer/goniometer, applying the standard sessile droplet technique with a droplet volume of approximately 2 μL. Each sample, placed within a glass chamber, was subjected to a gentle deposition of a water droplet. To enhance the visibility of the droplet, a homogeneous white light source was positioned behind the sample, rendering the droplet silhouette in stark contrast. Side-view images were captured using a charge-coupled device (CCD) camera to facilitate the subsequent analysis of the droplet's profile, which is indicative of the hydrophobic-hydrophilic balance of the NR hybrid films. The ambient conditions for the samples were controlled at a temperature of 22 ± 2 °C and a relative humidity of 48 ± 6% at the commencement of each experiment. The assessment of surface energy and its associated cellular interactions was predicated upon the contact angle measurements of liquids with varying polarities, interpreted through the lens of intermolecular forces specifically, polar and dispersive interactions. A minimum of five replicates were performed on disparate regions of each sample using water, with a polar surface tension component (γ_s^p = 51 mN m^{-1}, a dispersive component (γ_s^d = 21.8 mN m^{-1}, and a total surface tension (γ_s = 72.8 mN m^{-1}, and diiodomethane, with respective values of (γ_s^p = 0 mN m^{-1}, (γ_s^d = 50.8 mN m^{-1} and γ_s (CHF)= 50·8 mN m^{-1}). The surface energy of the substrate was computed based on the Owens-Wendt-Rabel-Kaelble method, which considers the polar γ_s^d and γ_s^p components of the free energy of the liquid interface.

In vitro experiments

A total of 120 wells containing Dulbecco's Modified Eagle Medium (DMEM) and osteoblasts, with n = 5 for each experimental group, were prepared to evaluate the morphological analysis, cell viability, and cell activity. Assessments were conducted at two time points: 48 h (n = 60) and 72 h (n = 60). The experimental groups were designated as follows: (*i*) control group with DMEM only; (*ii*) CHF group with films made from NR suspended in chloroform at a concentration of 10 mg mL^{-1}; (*iii*) CHF-CaP group with films made from NR and CaP in chloroform at a weight ratio of NR:CaP 5:1; (*iv*) TOL group with films made from NR suspended in toluene at a concentration of 10 mg mL^{-1}; (*v*) TOL-CaP group with films made from NR and CaP in toluene at a weight ratio of NR:CaP 5:1; (*vi*) CHF-Si group with films made from NR suspended in chloroform at a concentration of 10 mg mL^{-1} with negative SiP at 0.1 mg mL^{-1}; (*vii*) CHF-ASi group with films made from NR suspended in chloroform at a concentration of 10 mg mL^{-1} with positive SiP at 0.1 mg mL^{-1}; (*viii*) TOL-Si group with films made from NR suspended in toluene at a concentration of 10 mg mL^{-1} with negative SiP at 0.1 mg mL^{-1}; (*ix*) TOL-ASi group with films made from NR suspended in toluene at a concentration of 10 mg mL^{-1} with positive SiP at 0.1 mg mL^{-1}.

Culture of murine osteoblasts (OFCOL II)

Murine osteoblasts (OFCOL II) were obtained from the cell bank of the Federal University of Rio de Janeiro (BCRJ). The cells were cultured in Dulbecco's Modified Eagle Medium (DMEM) supplemented with 10% fetal bovine serum (FBS), 100 U mL^{-1} penicillin, 100 μg mL^{-1} streptomycin, and 100 U mL^{-1} amphotericin B as an antifungal agent. Cultures were maintained at 37 ºC in a humidified incubator with 5% CO_2. Cells between passages 18-20 were utilized for this study. For culturing, a 25 cm^3 flask was prepared by adding 1 mL of the cell stock to 4 mL of the enriched DMEM culture medium containing 10% FBS. The cells were incubated with automatic temperature control at 37 ºC and a regulated CO_2 atmosphere. Cellular growth was monitored using an inverted microscope (Nikon Eclipse TS100). Cells were subcultured upon reaching confluence. Trypsinization was performed by treating the cells with 2 mL of 0.05% trypsin for 3 min, followed by deactivation with 6 mL of DMEM culture medium supplemented with 10% FBS. Detachment from the flask surface was facilitated using a forceful stream from an automatic pipettor. The cell suspension was then transferred to a 15 mL conical centrifuge tube and centrifuged at 2000 rpm at 4 ºC for 5 min using a SOLAB SL-701 centrifuge. Subsequently, the supernatant was discarded, and the cell pellet was resuspended in 4 mL of complete medium. At least 1 mL of the cell suspension was used to inoculate new culture flasks. The medium was refreshed biweekly.

Cell morphology

Osteoblasts were examined under an inverted optical microscope (CKX41SF Olympus) after 48 and 72 h of incubation. Images were captured at 400× magnification for the following groups: DMEM, CHF, CHF-CaP, TOL, TOL-CaP, CHF-Si, CHF-ASi, TOL-Si, and TOL-ASi. A blinded descriptive analysis was conducted by two independent pathologists (VCCG, ACRML), who were unaware of the group assignments.

Cell viability

Cytotoxicity testing was conducted to evaluate the lethal

or sublethal effects of the produced films on cellular activity. The direct method utilizing the (3-(4,5-dimethylthiazol-2-yl)-2,5-diphenyl tetrazolium bromide) MTT assay was employed, which quantitatively measures mitochondrial function by reducing the tetrazolium component MTT to formazan. This reduction takes place within the mitochondria via the enzyme succinate dehydrogenase. As such, the quantity of formazan produced is directly proportional to the mitochondrial reduction capability of tetrazolium MTT. The assay was carried out using OFCOL II cells plated at a density of 3,000 cells *per* well in 96-well plates, each well containing NR hybrid films and 100 µL of culture medium. The cells were incubated for 48 and 72 h. Subsequent to these incubation periods, the culture medium was removed, leaving the films in place. To each well, 100 µL of MTT solution at a concentration of 1 mg mL^{-1} in complete culture medium were added. The plates were then incubated for 3 h at 37 °C in a 5% CO_2 atmosphere. Post incubation, 100 µL of the supernatant were carefully withdrawn and transferred to a new 96-well plate, followed by the addition of 100 µL of DMSO to each well. The plate was agitated for 30 s to ensure complete solubilization of the formazan crystals. Absorbance was measured using a spectrophotometer (Biotek) at 590 nm.

Cell activity

Alkaline phosphatase (ALP) is an enzyme present in various tissues, notably in higher concentrations within the liver and bones. In bone tissue, ALP is synthesized by osteoblasts the cells responsible for forming new bone playing a vital role in bone mineralization. Consequently, the activity of bone-specific ALP serves as an indicator of osteoblast activity. To assess this activity, supernatants were collected from the culture wells at 48 and 72 h following exposure to the NR hybrid samples. These supernatants were subsequently analyzed for bone-specific alkaline phosphatase activity using a commercial assay kit, following the laboratory protocol provided by the manufacturer (LABTEST®). This assay quantifies the enzyme activity by measuring the hydrolysis of *p*-nitrophenyl phosphate to *p*-nitrophenol, a process catalyzed by ALP. The procedure involved heating aliquots (100 µL) of each supernatant sample in a water bath at 56 ºC for 10 min to inactivate non-bone ALP isoforms, followed by immediate cooling in an ice bath. The thermostable fraction of ALP activity, which is indicative of non-bone isoforms, was measured directly at 30 ºC using a spectrophotometer set to an absorbance wavelength of 405 nm. The bone-specific ALP activity was then determined indirectly by subtracting the thermostable ALP activity from the total ALP activity measured in the samples.

Statistical analysis

Data are presented as the mean ± standard deviation (SD). Statistical comparisons of means were performed using one-way analysis of variance (ANOVA) followed by Tukey's *post-hoc* test. A *P*-value of less than 0.05 was considered indicative of statistical significance.

Results

Effects of the CaP incorporation on surface wettability and cell response

We initially characterized the impact of calcium phosphate (CaP) particle dispersion at the polymeric matrix on wettability and surface free energy of natural rubber (NR) films. Confocal microscopy images, as presented in Figure 1a, reveal the spatial distribution of CaP within the NR matrix, which predominantly exhibits micro-cluster formations with minimal individual particle isolation following hybridization. Figure 1b compares the contact angle measurements and surface free energy between NR samples incorporated with CaP, prepared with cyclohexane fluoride (CHF) and toluene (TOL) solvents, denoted as CHF-CaP and TOL-CaP, respectively. The key findings from our analysis of the reported results rendering this variable spectrum of contact angle values and surface free energy are twofold: (*i*) the choice of solvent significantly influences the surface wettability, with contact angle values being lower for TOL compared to CHF, and (*ii*) the incorporation of CaP particles does not substantially alter the surface wettability, as indicated by the lack of statistically significant changes in contact angle values and surface energy, suggesting the maintenance of stable wetting conditions. The choice of solvent was found to have a significant impact on the wettability of the coated surfaces. Samples processed with toluene (TOL) exhibited lower contact angle values compared to those prepared with chloroform (CHF), indicating improved wettability. Lower contact angles are associated with more hydrophilic surfaces, which enhance fluid spreading and interfacial interaction-key factors in biomedical applications such as catheter coatings, drug delivery systems, and tissue-contacting materials. In this context, the greater hydrophilicity achieved with TOL-based formulations suggests a more favorable surface profile for applications requiring reduced friction, enhanced biocompatibility, or improved adhesion of biological fluids and cells. The results support the notion that solvent selection plays a critical role not only in the morphological characteristics of the coating but also in determining surface energy and functional

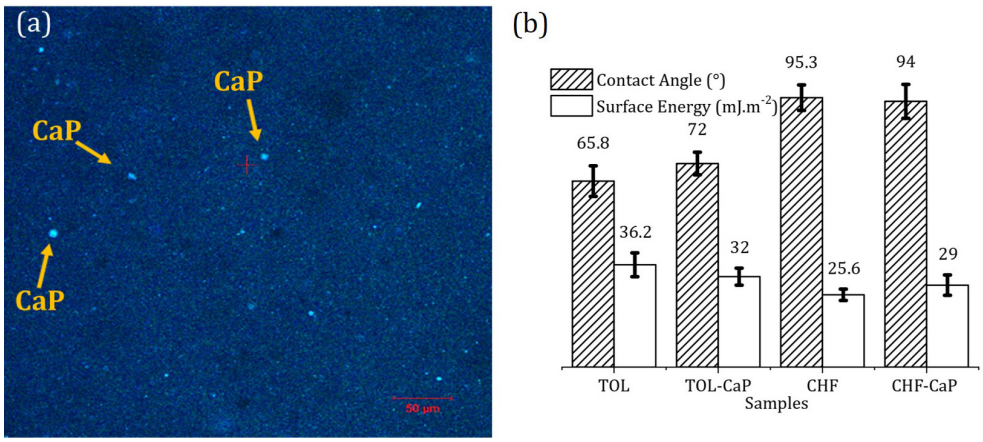

Figure 1. Physicochemical characteristics of the NR-CaP hybrid films: (a) confocal luminescence micrographs of the NR-CaP hybrid film. The NR-CaP auto fluorescence was induced by using a 405 nm laser. (b) Comparison of the contact angle and surface energy values before and after hybridization processes by CaP using TOL and CHF solvents.

performance. We subsequently assessed the influence of NR-CaP hybridization on cell viability.

Figure 2a shows the effects of natural rubber films from *Hevea brasiliensis*, dispersed in chloroform or toluene and with incorporated calcium phosphate, on murine osteoblasts's cell viability at 48 h. The results show that the addition of CaP does not affect the biocompatibility of NR, meaning that non-toxicity effects were observed. The NR films prepared with CHF solvent with incorporated CaP increased cell viability compared to DMEM and the NR films prepared with TOL ($P < 0.05$). The same effect was observed for groups CHF (i.e., films produced from NR chloroform suspension) and TOL (i.e., films produced from NR toluene suspension). Figure 2b shows the ALP activity of murine osteoblast cells on the NR films produced from CHF and TOL suspension. At 48 h, the cells in groups CHF and CHF-CaP presented higher ALP activity than DMEM ($P < 0.05$). The CHF group also showed a higher ($P < 0.05$) percentage of ALP activity when compared to the TOL and TOL-CaP groups. The CHF-CaP group presented a more elevated ($P < 0.05$) ALP activity percentage than the TOL and TOL-CaP groups.

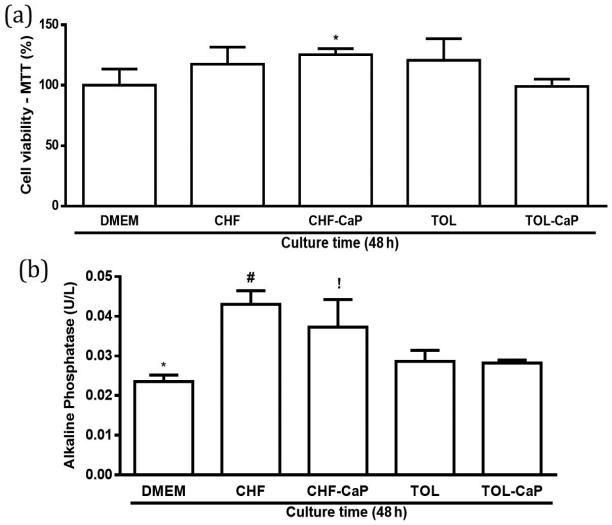

Figure 2. Effects on the (a) cell viability and (b) activity of alkaline phosphatase in murine osteoblast culture at 48 h induced by natural rubber films of *Hevea brasiliensis* dispersed in chloroform or toluene, incorporated or not with calcium phosphate. $^{*}P < 0.05$ for CHF-CaP compared to DMEM and TOL-CaP in (a). $^{*}P < 0.05$ for DMEM compared to CHF and CHF-CaP in (b). $^{\#}P < 0.05$ for CHF compared to TOL and TOL-CaP in (b). $^{!}P < 0.05$ for CHF-CaP compared to TOL and TOL-CaP in (b).

Effects of the incorporation of positively and negatively charged SiP in NR on the surface wettability and cell response

Figure 3a shows the confocal microscopy images of the NR-SiP hybrid films excited by a 488 nm laser source. The imaging reveals distinct spatial distributions that correlate with the charge of the particles. Negatively charged SiPs exhibit a heterogeneous distribution within the CHF-Si and TOL-Si matrices, forming sparse aggregates as depicted in Figures 3c and 3d. In contrast, positively charged SiPs demonstrate a homogeneous distribution in CHF-ASi and TOL-ASi. Figure 3e illustrates the contact angle measurements and the corresponding surface free energy of the NR matrices, both in the presence and absence of CHF and TOL, as well as the hybrid NR-SiP samples with charged SiPs. The incorporation of positively charged SiPs markedly enhances the hydrophilicity of the NR surface, evidenced by the decrease in contact angle from approximately 94° to 68°. This suggests a predominant influence of the polar component over the dispersive energy component, the former being indicative of modifications in dipole moments, whereas the latter corresponds to charge fluctuations due to long-range intermolecular forces. Concurrent with the decreased contact angle, there

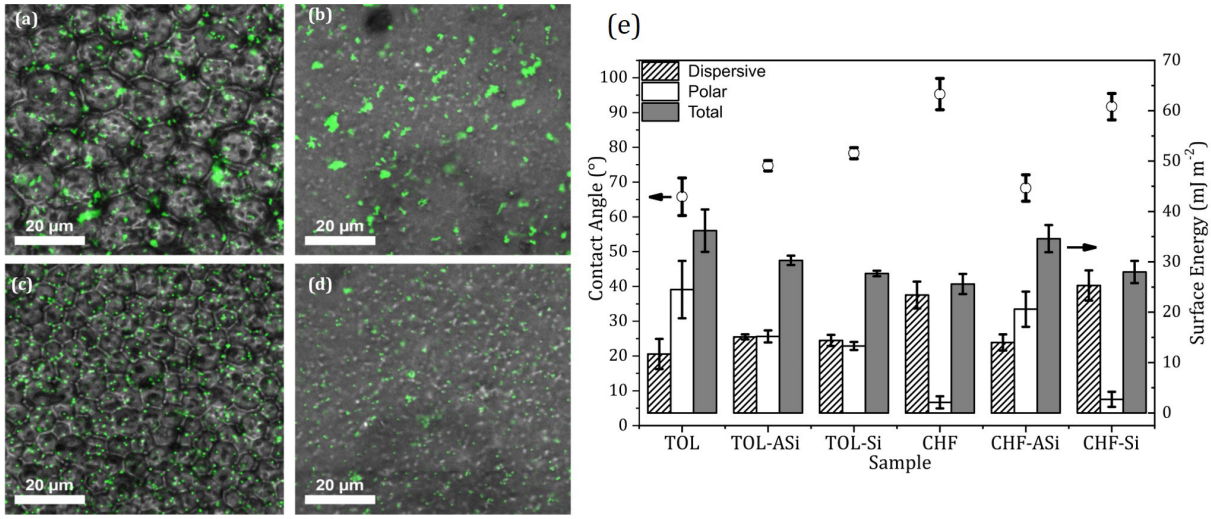

Figure 3. Physicochemical characteristic of the NR-SiP hybrids. Confocal luminescence micrographs of the NR-SiP hybrid films (a) CHF-Si, (b) CHF-ASi, (c) TOL-Si, and (d) CHF-ASi. Mapping was performed using spectroscopic and microscopic characterization of the samples using the SiPs as *in situ* fluorescent probes. The NR autofluorescence and NR-SiP particles cores were excited using a 488 nm laser. Comparison of the contact angle and surface energy values before and after hybridization processes by SiP using TOL and CHF solvents (e).

is observed elevation in the polar component, signifying increased hydrophilicity of the surface. Conversely, the dispersive component appears invariant in TOL samples, regardless of SiP incorporation.

Figure 4a depicts the cell viability of murine cells cultured *in vitro* at the 48-h mark. The assessment of Si particles' cell viability indicated no significant difference among the groups ($P > 0.05$) after 48 h. As demonstrated in Figure 4b, the CHF group presented a significantly higher level of alkaline phosphatase (ALP) activity compared to the CHF-Si, CHF-ASi, TOL, and TOL-ASi groups during the same period ($P < 0.05$). Additionally, the TOL-Si group exhibited a notably increased ALP activity relative to the TOL, TOL-ASi, and CHF-Si groups ($P < 0.05$).

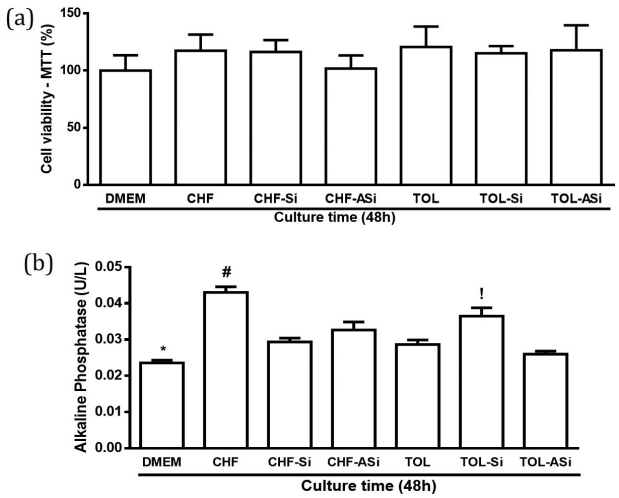

Figure 4. Effects of natural rubber films from *Hevea brasiliensis*, dissolved in chloroform or toluene and filled with silica particles, on cell viability (a) and alkaline phosphatase (ALP) activity (b) *in vitro* culture of murine osteoblasts at 48 h in the following groups: DMEM, CHF, CHF-Si, CHF-ASi, TOL, TOL-ASi and TOL-Si. (a) The groups: DMEM, CHF, CHF-Si, CHF-ASi, TOL, TOL-Si, TOL-ASi. $^{*}P < 0.05$ DMEM *versus* CHF, CHF-Si and TOL-Si. $^{\#}P < 0.05$ CHF *versus* CHF-Si, CHF-ASi, TOL and TOL-ASi. $^{!}P < 0.05$ TOL-Si *versus* CHF-Si, TOL and TOL-ASi (b).

Effects of hybridization of the NR on cell morphology *in vitro* culture of murine osteoblasts

Figure 5 shows optical micrographs of osteoblastic cells seeded on different surfaces for 48 and 72 h. At 48 h, osteoblasts from groups DMEM, CHF, and TOL were elongated. The varying morphologies of cells observed in the images can arise from a range of processes, including local surface variations due to material engineering, and biological heterogeneity, which encompasses differences in viabilities, differentiation, or other variable biological states. In general, osteoblasts cultivated in NR films incorporated with CHF-CaP or TOL-CaP revealed cell proliferation and contact area. The morphology of osteoblasts on NR-SiP hybrids (CHF-ASi, CHF-Si, TOL-ASi, TOL-Si) were elongated in shape, but more dead osteoblasts than differentiated ones were observed. On the other hand, in the TOL-ASi group, some osteoblasts displayed contact areas.

By the 72-h mark, there was an enhancement in osteoblast proliferation across nearly all groups, with cells displaying a spindle shape. NR films containing CHF-CaP, TOL-CaP, or TOL-CaP demonstrated a uniform distribution of cells on surfaces suggesting relatively low cell adhesion. Within the NR-SiP hybrid groups (CHF-ASi, CHF-Si, TOL-ASi, TOL-Si), osteoblastic cells also appeared elongated, yet exhibited a noticeable decrease in spreading, with no discernible contact area among them.

The incorporation of CaP into the NR matrix improved the osteoblast proliferation stage regardless of the solvent used. This observation may be attributed to the enhanced cell adhesion facilitated by polar and dispersive components of the surface free energy, particularly evident in the CHF-CaP and TOL-CaP groups.

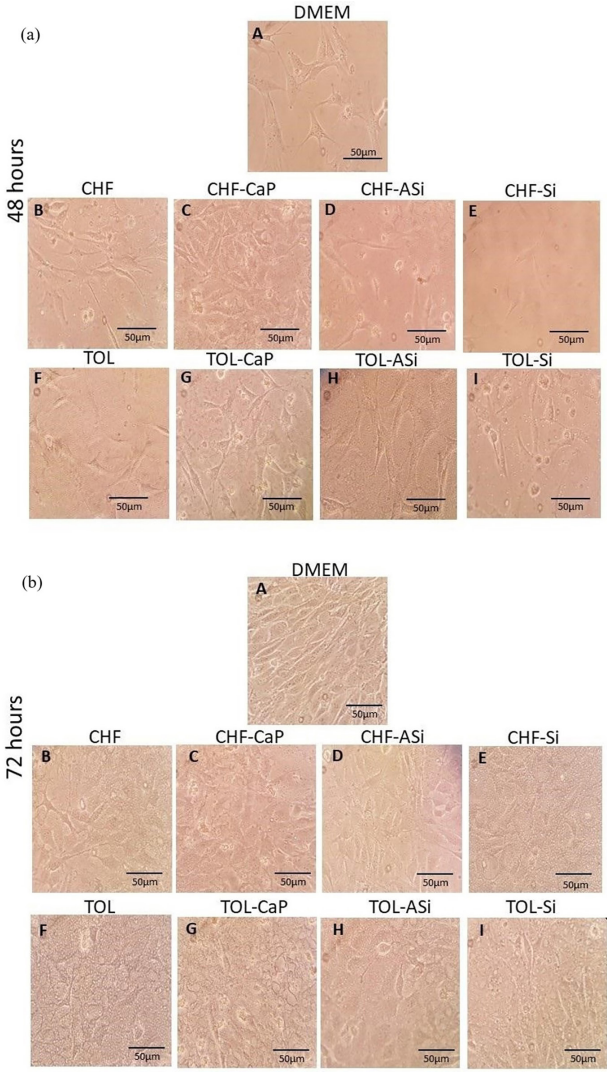

Figure 5. Images from *in vitro* culture of murine osteoblasts at (a) 48 and (b) 72 h. Morphology of osteoblasts are shown in the following groups: DMEM (A), CHF (B), CHF-CaP (C), CHF-ASi (D), CHF-Si (E), TOL (F), TOL-CaP (G), TOL-ASi (H) and TOL-Si (I). Scale bars = 50 µm.

From the above, it can be seen that the biocompatibility of the NR-CaP and NR-SiP hybrid films, irrespective of solvent medium, was conclusively affirmed. We observed that the hybrids exhibited either homogeneous or heterogeneous distributions within the NR matrix, leading to a variance in surface wettability contingent upon the specific amalgamation of SiP, CaP, chloroform (CHF), and toluene (TOL). Furthermore, the study establishes that the NR hybridization process significantly impacts on osteoblast proliferation, activity, and morphology. It becomes evident that cellular responses are contingent on the choice of solvent and the intrinsic properties of the inorganic particles. The interaction between these variables yielded differential levels of biocompatibility.

Discussion

The hybridization of NR with the incorporation of functional particles opens up new possibilities for the creation of materials suited to biomedical applications. A fundamental prerequisite for advancing such biomedical applications is to elucidate the relationship between physicochemical alterations of NR properties and the resultant cellular interactions when various fillers are integrated into the matrix. This understanding is critical as it underpins the design of the material tailored to specific biomedical functions, potentially enhancing biocompatibility and cellular response.

We synthesized two NR hybrid systems to investigate physicochemical changes induced by inorganic fillers-CaP and silica SiP. The goal was to evaluate how hybridization affects osteoblast behavior, relevant to bone regeneration in advanced biomedicine. We first analyzed solvent effects, comparing chloroform and toluene, both common NR dispersants. Then, we assessed how CaP and SiP influence key surface features-wettability and surface energy-critical for cell adhesion.

Structural rearrangements in the polymeric matrix of NR films can be attributed to the choice of solvent used for dispersion and the type of particles incorporated. These alterations may significantly affect the surface properties of the films, notably their wettability. The contact angle measurements indicate that the wetting behavior of NR hybrids is influenced by the solvent employed during processing rather than the integration of calcium phosphate (CaP) as shown in Figure 1. In contrast, a distinct behavior is observed for NR-SiP hybrids. The introduction of positively charged silica (ASi) alters the surface energy, leading to reduced wettability as demonstrated in Figure 3. These changes may result from modifications in topology, surface energy, or a combination of both. Surface energy is predominantly governed by polar and dispersive interactions. Detailed analysis of the hybridization effects on energy components revealed that the wetting regime undergoes a modification, predominantly due to an increase in polar interactions. This could be ascribed to the mobilization of intrinsic charges within the particles in NR. It is important to note that both the choice of solvent and the inclusion of particles play a role in modifying the components of the free surface energy of the polymer.

The influence of solvents used in material processing on cellular response was investigated to understand their role in materials science and engineering, as well as in biomedical applications. Cell viability assays conducted with NR films containing calcium phosphate (CaP) and dispersed in various solvents revealed differential outcomes (see Figure 2). After 48 h, an enhancement in cell viability was noted in the group where NR-CaP was processed with chloroform (CHF-CaP). Conversely, the toluene (TOL) and (TOL-CaP) groups exhibited a decrease in cell viability, implying a potential cytotoxic effect of NR films when dispersed in toluene, irrespective of CaP incorporation. Consequently, Figure 1b delineates our findings, endorsing chloroform as a preferred solvent for NR processing in the synthesis of hybrids with CaP. This preference is due to chloroform's facilitation of film size and uniformity, along with the maintenance of a stable wetting regime and surface energy.

The solvent choice significantly impacts the biocompatibility of NR hybrid systems. Our studies indicate that hybrids processed with chloroform (CHF) exhibit diminished toxicity and enhanced cell proliferation. Specifically, the addition of calcium phosphate (CaP) to NR films obtained from chloroform correlates with increased cell viability, particularly in the CHF-CaP group. This improved viability persists for 72 h, despite a noted decrease in the parameter over time. The observed decrease might be attributable to alterations in the cell microenvironment, potentially influenced by the charge properties of silica particles (SiP) present in the system.

Alkaline phosphatase activity (ALP), a pivotal marker for osteogenic differentiation, viable osteoblast activity, and neo-osseous matrix production, was quantitatively measured to provide a comprehensive cell-substrate interaction assessment. Over the course of 48 and 72 h, ALP expression was enzymatically evaluated to elucidate the osteogenic influence of NR hybrid systems *in vitro*. An enhancement in ALP activity at the 48-h mark was observed within the chloroform groups, inclusive of the calcium phosphate-incorporated subset (CHF-CaP).

Furthermore, our findings demonstrated an augmentation in ALP activity associated with the incorporation of negatively charged silicate particles (SiP) into the toluene-based groups (TOL-Si). Corroborating with established studies, SiP is known to influence osteoblastic metabolic activity and type I collagen synthesis, thereby modulating bone cell metabolism and mineralized tissue formation.[27] Thus, our data suggest that SiP integration exerts a regulatory effect on bone homeostasis. In conclusion, our investigation highlights a significant upregulation of ALP activity in the context of NR hybrid systems, underscoring their potential utility in the field of bone tissue regeneration.

The attached osteoblasts on hybrid NR systems exhibit various morphologies, as depicted in the accompanying images of the Figure 5. Some cells maintain a spherical shape, indicating limited interaction with the surface. Conversely, other cells display extensive spreading, characterized by the formation of branches at the micron scale. This enhanced spreading is indicative of robust adhesion and engagement with the substrate. Cell attachment involves a complex process known as adhesion-deformation. Under favorable conditions, this process gradually transforms the original spherical and detached cell shape into a spread-out form on the material surface. This transformation occurs through a combination of passive and active mechanisms. Passive mechanisms involve physical forces such as van der Waals interactions, while active mechanisms include biochemical processes mediated by cell surface receptors. Furthermore, the formation of a 'cell carpet' structure, resembling monolayers, is noteworthy. This process involves the establishment of intimate contacts between neighboring cells, leading to the assembly of a cohesive tissue-like structure. Such monolayers play a crucial role in tissue integration and assembly, facilitating the establishment of functional tissue interfaces and promoting biological responses such as cell signaling and differentiation.

Our results accentuate the role of inorganic particle fillers in enhancing the functionality of these hybrid systems, thus supporting the development of (nano) material-based therapeutic strategies for bone tissue regeneration. Nonetheless, despite the valuable and reproducible results obtained from the selected cell type (osteoblasts) and bone marker (ALP), the intricacies of bone healing processes demand comprehensive *in vivo* studies to validate these findings and fully ascertain their clinical relevance.

Conclusions

The unique composite properties of the NR composites accentuate their potential as significant contributors to the field of biomaterials and medicine. The incorporation of different particles into NRHS allowed control over surface energy and wettability, which are crucial for biocompatibility. Depending on the chosen solvent-particle system, the materials could sustain, hinder, or improve osteoblast proliferation and enzymatic activity-both NR-CaP and NR-SiP composites modified surface properties without compromising cell viability. As we look ahead, the heterogeneity in cell responses presents a compelling directive for further investigation, prompting in-depth studies to optimize these systems for clinical applications. Overall, the findings demonstrate that NRHS can be tailored

through particle addition, showing promising applicability in biosensors and biomedical devices.

Acknowledgments

The authors acknowledge CNPq for grants 423567/2018-7 and 309454/2021-2, and Ceará State Research Funding Agency (FUNCAP) for grant PRONEM PNE-0112-000480100/16.

Data Availability Statement

Additional data can be obtained upon request from the corresponding author.

Author Contributions

L. M. S. was responsible for study conception, conceptualization, methodology, investigation, and writing the original draft; R. M. N. for study conception, data curation, formal analysis, writing of the original draft, and support with conceptualization; N. C. O., R. F. C. L., F. A. C. R., and A. J. P. for provision of samples and material resources; A. C. R. M. L. and M. M. B. for formal analysis and critical review of the original draft; B. O. L. for review, formatting, and editing of the original draft; V. C. C. G.-C. for conceptualization and supervision.

References

1. Rippel, M. M.; Galembeck, F.; *J. Braz. Chem. Soc*. **2009**, *20*, 1024. [Crossref]
2. Niamlang, I.; Pavasupree, S.; Boonchu, N.; Sirivat, A.; *Mater. Today: Proc.* **2017**, *4*, 6267. [Crossref]
3. Gao, J.; He, Y.; Gong, X.; *Results Phys.* **2018**, *9*, 493. [Crossref]
4. Li, J.; Zhao, X.; Zhang, Z.; Xian, Y.; Lin, Y.; Ji, X.; Lu, Y.; Zhang, L.; *Compos. Sci. Technol.* **2020**, *186*, 107930. [Crossref]
5. Andrade, K. L.; Faita, F. L.; do Nascimento, R. M.; Cunha, R. S.; Bresolin, D.; Acosta, E. D.; Machado, R. A. F.; *Surf. Interfaces* **2022**, *32*, 102129. [Crossref]
6. Chen, X.; Qiu, T.; *Polym. Test.* **2020**, *81*, 106271. [Crossref]
7. Zhang, G.; Wang, J.; *J. Phys. Chem. Solids* **2018**, *115*, 137. [Crossref]
8. Chen, X.; Qiu, T.; Christoforo, T.; Wei, W.; Liang, J.; Wei, Y.; *ACS Appl. Mater. Interfaces.* **2022**, *14*, 55155. [Crossref]
9. Giovanetti, K.; Tuma, R. B.; Brasil, G. S. P.; Miranda, M. C. R.; Borges, F. A.; Tanaka, J. L.; Burd, B. S.; Cortellazzi, K. L.; Guerra, N. B.; Mussagy, C. U.; Floriano, J. F.; dos Santos, L. S.; Silva, W. M.; Cao, W.; Herculano, R. D.; Caria, P. H. F.; *Int. J. Biol. Macromol*. **2024**, *282*, 137328. [Crossref]
10. Gittens, R. A.; Scheideler, L.; Rupp, F.; Hyzy, S. L.; Geis-Gerstorfer, J.; Schwartz, Z.; Boyan, B. D.; *Acta Biomater.* **2014**, *10*, 2907. [Crossref]
11. do Nascimento, R. M.; Rodrigues, J. E. F. S.; Favarin, B. Z.; Ramos, A. P.; Ciancaglini, P.; Pecharroman, C.; Rahouadj, R.; Hernandes, A. C.; Bechtold, I. H.; *Surf. Interfaces.* **2022**, *31*, 102048. [Crossref]
12. do Nascimento, R. M.; Schmitt, J. F.; Sarig, U.; Rodrigues, J. E. F. S.; Pecharromán, C.; Ramos, A. P.; Ciancaglini, P.; Faita, F. L.; Rahouadj, R.; Hernandes, A. C.; Bechtold, I. H.; *Langmuir* **2021**, *37*, 4639. [Crossref]
13. Florian, F.; Guastaldi, F. P. S.; Cominotte, M. A.; Pires, L. C.; Guastaldi, A. C.; Cirelli, J. A.; *J. Mater. Sci: Mater. Med*. **2021**, *32*, 57. [Crossref]
14. Shiwaku, Y.; Tsuchiya, K.; Xiao, L.; Suzuki, O.; *J. Biomed. Mater. Res. A* **2019**, *107*, 1001. [Crossref]
15. Chan, A. J.; Steenkeste, K.; Canette, A.; Eloy, M.; Brosson, D.; Gaboriaud, F.; Fontaine-Aupart, M. P.; *Langmuir* **2015**, *31*, 12437. [Crossref]
16. Prasertsri, S.; Rattanasom, N.; *Polym. Test*. **2011**, *30*, 515. [Crossref]
17. Prasertsri, S.; Lagarde, F.; Rattanasom, N.; Sirisinha, C.; Daniel, P.; *Polym. Test*. **2013**, *32*, 852. [Crossref]
18. Peng, Z.; Kong, L. X.; Li, S. D.; Chen, Y.; Huang, M. F.; *Compos. Sci Technol*. **2007**, *67*, 3130. [Crossref]
19. Oliveira, N. C.; Paula, A. J.; Maia, M. T.; Noronha, V. T.; Alves, A. C.; Freire, R. M.; Souza Filho, A. G.; Ferreira, O. P.; Faria, A. F.; do Nascimento, R. M.; *ACS Appl. Nano Mater*. **2022**, *5*, 14492. [Crossref]
20. Arnoldussen, Y.J.; Ervik, T. K.; Eriksen M. B.; Kero, I.; Skaug, V.; Zienolddiny, S.; *Int. J. Mol. Sci.* **2019**, *20*, 358. [Crossref]
21. Uribe, P.; Johansson, A.; Jugdaohsingh, R.; Powell, J. J.; Magnusson, C.; Davila, M.; Westerlund, A.; Ransjö, M.; *Sci. Rep*. **2020**, *10*, 9923. [Crossref]
22. Xu, Y.; Jiang, Y.; Xia, C. S.; Wang, Y.; Zhao, Z.; Li, T.; *Regener. Ther*. **2020**, *15*, 295. [Crossref]
23. Venkatesan, J.; Anil, S.; Kim, S. K.; Shim, M. S.; *Int. J. Biol. Macromol*. **2017**, *104*, 1383. [Crossref]
24. Nascimento, R. M.; Faita, F. L.; Agostini, D. L. S.; Job, A. E.; Guimarães, F. E. G.; *Mater. Sci. Eng. C* **2014**, *39*, 29. [Crossref]
25. Maia, M. T.; Noronha, V. T.; Oliveira, N. C.; Alves, A. C.; Faria, A. F.; Martinez, D. T. S.; Ferreira, O. P.; Paula, A. J.; *ACS Appl. Nano Mater*. **2022**, *5*, 4634. [Crossref]
26. Ho, C. C.; Kondo, T.; Muramatsu, N.; Ohshima, H.; *J. Colloid. Interface Sci*. **1996**, *178*, 442. [Crossref]
27. Fu, Y.; Cui, S.; Luo, D.; Liu, Y.; *Nanomaterials* **2021**, *11*, 789. [Crossref]

Submitted: August 30, 2025
Final version online: November 6, 2025